Application of the small punch test to evaluate the integrity of a cold spray titanium coating

A. Wong [1], Y.L. Tan [1], M. Pilot [1], R.J. Lancaster [1], S.P. Jeffs [1], F. Li [2], A.W.Y. Tan [3], W. Sun [3], E. Liu [3], I. Mitchell [4]

[1] Institute of Structural Materials, Swansea University, Bay Campus, Swansea, UK, SA1 8EN
[2] Rolls-Royce Singapore, 1 Seletar Aerospace Crescent, 797565 Singapore
[3] Nanyang Technological University, 50 Nanyang Ave, Singapore
[4] Rolls-Royce plc., P.O. Box 31, Derby, UK, DE24 8BJ
* Correspondence: r.j.lancaster@swansea.ac.uk; Tel.: +44-1792-295965

Abstract: Metal Cold Spray (MCS) is currently under evaluation for its suitability for aerospace applications. However, before this technology can be implemented into the jet engine, the mechanical performance and structural integrity of this novel process must be fully understood. Limited data is currently available to determine key materials properties given the discrete and transient nature of a MCS component. Furthermore, it is extremely challenging to produce uniaxial test coupons that are truly representative of the in-service geometry. As such, the small punch (SP) test offers an attractive alternative, since miniature disc SP specimens can be extracted from localised discrete locations. This paper will report the findings from an experimental collaborative programme of work currently being undertaken by Swansea University, Rolls-Royce Singapore and Nanyang Technological University Corp Lab to understand the contrasting modes of failure in a Ti-6Al-4V coating sprayed on to a Ti-6Al-4V substrate, which is expected to have properties akin to a forged variant. This will include a series of SP tests to assess the integrity and performance across the substrate, bond line and coating. Results will be supported by additional microstructural and fractographic investigations.

1. Introduction

Performance, cost and time are among the main drivers of material technology in the aerospace industry. As novel materials and processes are developed and incorporated in gas turbine engines, repair technologies are evolving simultaneously to ensure that aerospace components can still operate in optimal condition during service in a cost-effective approach. Traditional repair methods such as welding or hot spraying can lead to a number of deleterious effects on the component being repaired. These include the formation of heat affected zones, residual stresses, oxidation and porosity [1]. Furthermore, the deposition of sufficiently thick coatings is prohibited by thermal stresses generated within the component [2]. These effects can potentially reduce the service life of components and lead to premature failure.

In light of these issues, cold gas dynamic spray (or cold spray) offers a promising alternative that could alleviate the shortcomings caused by high temperature repair processes. Cold spray is a solid-state material deposition process where micron-sized particles are sprayed onto substrates at temperatures below the melting point of the metallic particles and under supersonic velocities [3]. Particle-substrate and particle-particle bonds are formed via mechanisms pertaining to adiabatic shear instabilities of particles upon impact rather than high temperatures [1, 3]. The name of this process is derived from the fact that the feedstock powder material remains solid during the process, which is different from conventional thermal spraying methods, where particles are partially or entirely molten as they impinge on the substrate [3]. Besides avoiding the aforementioned drawbacks, cold spray is cost effective as it offers short processing times [4]. Detailed explanations of the cold spray process can be found in [1, 3].

In order to evaluate the quality of repair methods, mechanical test techniques for assessing the structural integrity of materials are a critical aspect to consider. Although conventional approaches such as the uniaxial tensile test, Charpy impact test and fatigue test are well standardised, they still contain a number of inherent limitations. For instance, they require a sufficiently large volumes of material for the specimens to be machined to certain specifications, which can pose a problem if there is limited material availability. They also sometimes fail to capture the local microstructural effects during testing due to geometric constraints in the component [5]. Therefore, miniaturised test techniques such as the small punch (SP) test have been developed to address these issues. This

technique is a research topic of great interest to the scientific community, due to its ability to assess the mechanical behaviour of materials in small volumes. However, there is very little published literature describing the use of SP test as a means to assess the mechanical properties of cold-sprayed metal specimens. This paper aims to report results from the characterisation of mechanically tested Ti-6Al-4V MCS samples using SP testing. Of particular interest are the contrasting failure modes of samples when they are tested at different loads, times and temperatures, and the microstructural evolution across the bondline and into the coating. Experimental results from mechanical tests are further elucidated with the use of optical and scanning electron microscopy to identify important fractographic features such as the crack origin and propagation route. Characterisation results will also be compared for different test parameters.

2. Materials and Methods

2.1. Material

The material used in in this study originated from rectangular blanks with a Ti-6Al-4V coating thickness of 1.5mm and a Ti-6Al-4V substrate thickness of 4.2mm. A schematic illustration of the cold spray apparatus is shown in Figure 1. In the following step, cylindrical rods with a 9.5mm diameter were extracted from these blanks. These specimens were then sectioned into slices with a thickness of approximately 0.7-0.8mm. In order to prepare specimens according to guidelines provided in the European Code of Practice (EUCoP) for Small Punch Testing [6], the slices were ground and polished to a specimen thickness of 0.5mm ± 0.005mm with progressively finer grades of silicon carbide (SiC) abrasive paper. A final grade of 1200-grit was used to achieve a polished surface finish. Additionally, as-sprayed samples were sectioned from the remnants of the rectangular blanks for material characterisation.
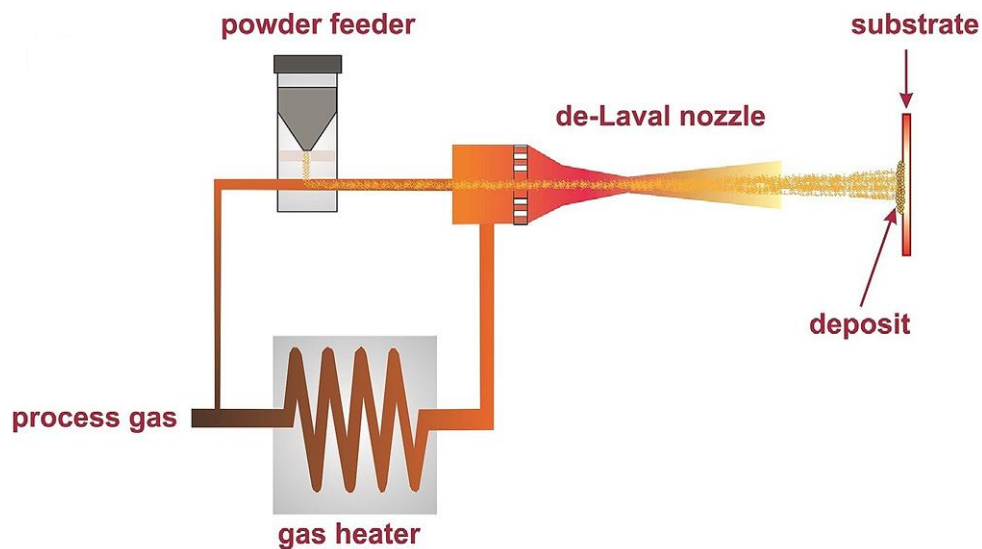

Figure 1. Schematic diagram of cold spraying apparatus [3].

2.2. Small Punch Tensile Testing

SP tensile tests were conducted using a bespoke test jig manufactured from Nimonic-90, housing both the SP disc specimen and the hemispherical indenter punch, as shown in Figure 2. The tensile test jig consists of an upper and lower die with a receiving hole of 4mm diameter, designed to clamp the miniature disc specimen in place. The specimen is punched from above by an indenter with a hemispherical tip of 2.5mm diameter aligned perpendicular to the flat upper surface of the specimen. SP tensile tests were conducted at constant displacement rates of 0.5mm·min^{-1}, all of which are within the EUCoP recommended range of 0.2mm·min^{-1} to 2mm·min^{-1} [6]. The specimens used for SP tensile test are classified according to their microstructure. Samples C, C2 and C3 are those with the coating layer only, while samples S, S2 and S3 consist of the substrate layer only. Samples B, B2 and B3 are taken from across the bondline, where the coating and substrate content is approximately equal. For convenience, samples denoted by B (i.e. B, B2 and B3) will be referred to as bondline samples, those denoted by S referred to as substrate and those denoted by C referred to as coating. Substrate and coating sample were tested only at 600 K,

whereas bondline samples were tested at 3 different temperatures: room temperature, 600 K and 650 K. All bondline specimens were tested with the punch in contact with substrate surface. The room temperature tests were carried out in a controlled laboratory environment at 20°C ± 2°C. During the elevated temperature tests, temperature was monitored using a Type N thermocouple, which was inserted into the jig from below through a hollow quartz rod in contact with the specimen. The deflection of the specimen was measured using a linear variable displacement transducer (LVDT). The LVDT was located directly below the underneath of the disc and maintained contact with the specimen via the quartz rod [7].
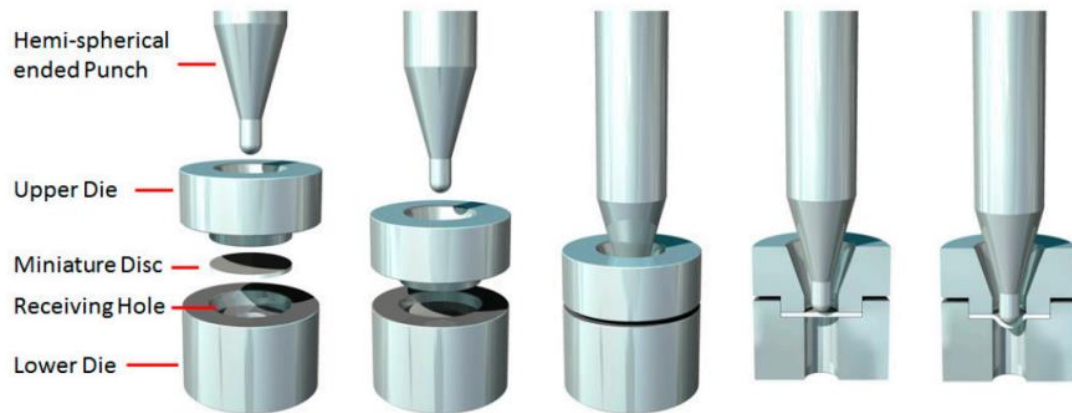

Figure 2. Small punch tensile test apparatus.

2.3. Microscopy

Microstructural characterisation of the SP and as-sprayed samples were performed using a Keyence VHX-700FE digital microscope and a Hitachi SU3500 scanning electron microscope (SEM). In the first instance, the Keyence was used to obtain plan view micrographs from the top, side and bottom surfaces of the SP samples. Secondary electron (SE) imaging mode in the SEM was used to analyse the failure modes, volume fraction and general microstructure of samples used in this study. Furthermore, the porosity in the as-sprayed samples were studied using a Zeiss Smartzoom 5 digital microscope, and post-analysis was performed using ImageJ.

3. Results and Discussion

3.1. Small Punch Tensile Testing

SP test results at 600 K are provided in Figure 3. The pure substrate samples showed the highest average maximum load of 1.44 kN. The bondline samples showed moderate strength with an average maximum load at 0.99 kN, whereas the coating samples showed the lowest average of 0.36 kN. A potential cause for the reduced performance in the coating samples is the population of porosity found in this variant. The presence of porosity tends to allow cracks to propagate more easily across the powder particles and can act as internal stress raisers, reducing the integrity of the material. In contrast, substrate samples can sustain a higher load as the number of porosity sites are expected to be minimal. A more detailed investigation on the levels of the porosity in each of the specimens will be discussed later in the paper. Since bondline samples consist of coating and substrate layer, they have moderate strength as compared to pure substrate or pure coating samples.

The displacement at failure values shown on each graph give an estimation of the ductility across the three locations. The results suggest that the coating samples showed the most brittle behaviour, while the substrate samples showed reasonable ductility. Bondline samples displayed the most ductile behaviour, as evidenced by the significant amounts of deflection achieved prior to failure.
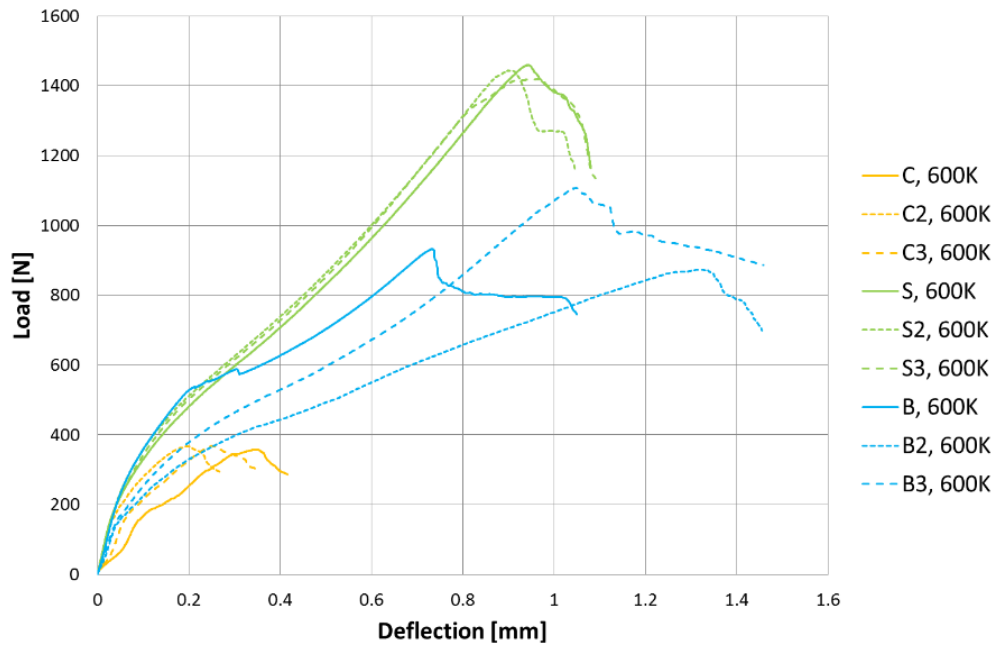
Figure 3. Collation of SP test load-displacement data for coating, substrate and bondline specimens at 600K with a displacement rate of $0.5\text{mm}\cdot\text{min}^{-1}$.

SP test results for bondline samples are shown in Figure 4. Although the bondline samples were all tested under the same conditions, the corresponding load-displacement curves showed considerable differences. The variation in the results can be attributed to the differing fractions of substrate and coating layers in these samples. For example, the peak load for sample B3 is significantly higher than that for samples B and B2 when they were tested at 600 K (see black arrows in Figure 4). According to Table 1, the percentage of substrate thickness for sample B3 (i.e. 90%) is much higher than that for the percentage of coating thickness (i.e. 10%). In contrast, the percentage of substrate thickness for sample B2 (i.e. 60.2%) is only slightly higher than the percentage of coating thickness (i.e. 39.8%). Therefore, a higher proportion of substrate will confer more strength to the bondline samples. Another important observation can be made when the test temperature is varied. The bondline sample tested at 650 K (i.e. B3) gave a peak load of 0.89 kN, whereas sample B2 tested at 600 K had a slightly lower peak load of 0.87 kN. However, when tested at room temperature, the bondline sample (i.e. B3) achieved a much lower peak load of 0.72 kN. These observations suggest that the ductility of bondline samples increase with temperature, hence they are able to deflect more and bear higher loads.
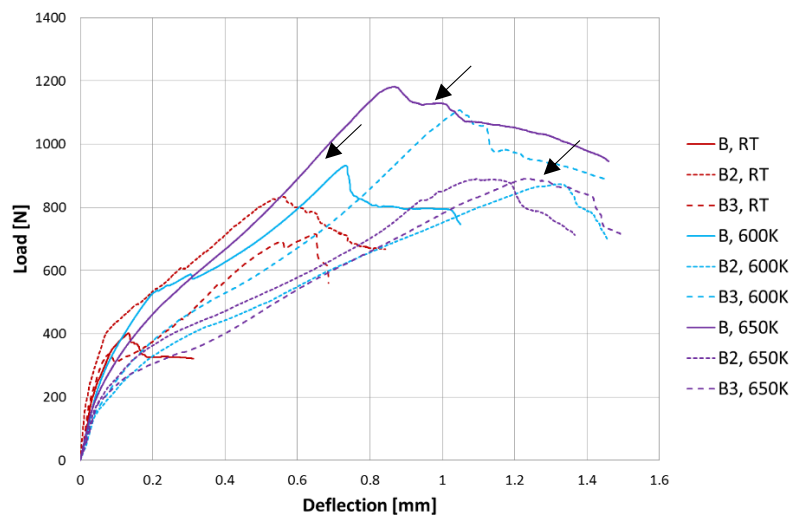

Figure 4. Collation of SP test load-displacement data for bondline specimens at room temperature, 600 K and 650 K with a displacement rate of $0.5\text{mm}\cdot\text{min}^{-1}$.

Table 1. Volume fraction calculation of bondline specimen.

Sample number	Percentage Thickness (%)	
	Coating	Substrate
BONDLINE RT		
B (10)	100.0	0
B2 (29)	37.6	62.4
	37.0	63.0
*B3 (12)	48.8	51.2
	44.2	55.8
BONDLINE 600K		
B (13)	55.0	45.0
	44.0	56.0
*B2 (14)	51.4	48.6
	39.8	60.2
B3 (15)	10.0	90.0
	20.2	79.8
BONDLINE 650K		
B (25)	31.4	68.6
	17.0	83.0
B2 (26)	39.0	61.0
	52.8	47.2
*B3 (27)	46.8	53.2
	45.8	54.2

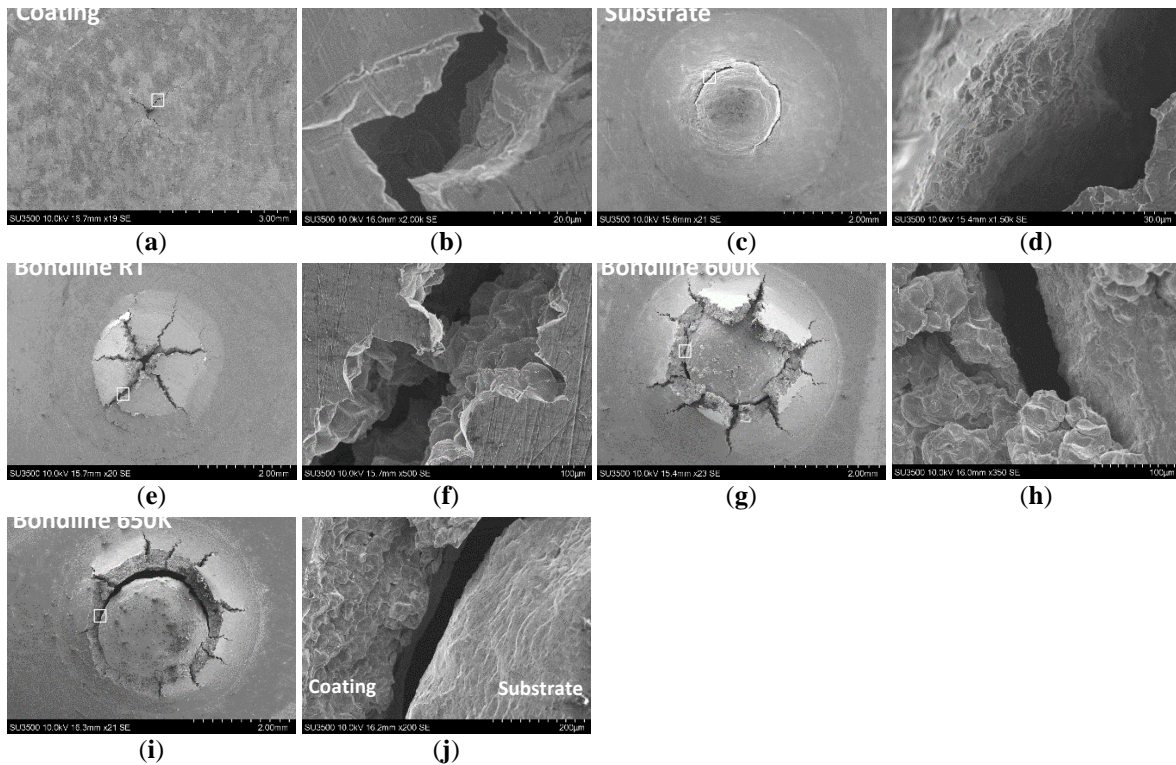*Samples B3(12), B2(14) and B3(27) were selected for further investigation*

Figure 5. Macroscopic and microscopic micrographs of disc fracture surfaces from SP tests: (**a,b**) coating specimen at 600K, C3; (**c,d**) substrate specimen at 600K, S; (**e,f**) bondline specimen at RT, B3; (**g,h**) bondline specimen at 600K, B2; (**i,j**) bondline specimen at 650K, B3.

The fracture surfaces of coating C3(2), substrate S(5), and bondline samples B3(12), B2(14) and B3(27) are shown in Figure 5. Based on their appearance, these samples showed distinct differences in their deformation behaviour. The coating sample (Figure 5a,b) shows a flat crack surface without much evidence of plastic deformation. When viewed at a higher magnification, facets can be observed on the crack surface, which suggests

that it failed in a brittle manner. In contrast, the dominant circumferential crack on the substrate sample (Figure 5c,d) is evidence of a typically ductile failure. A dimple fracture is observed due to the formation of micro-voids which then grow and coalesce, suggesting the occurrence of ductile tearing during disc rupture [8, 9].

For the bondline samples, images were taken on the underneath of the sample, capturing the deformation of the coating since the punch was imparted onto the substrate layer of the disc. On the macro scale, a star-shape crack is observed in the bondline specimens across all three temperatures (Figure 5e,g,i). As the temperature increases, the coating layer tends to detach from the sample. This could be due to the fact that at a higher temperature, the substrate layer tends to be more ductile which creates more deflection towards to the coating layer. Furthermore, at higher temperatures, the coating layer is expected to be more rigid and the powder particles are packed more closely together as the number of porosity sites may be reduced, thereby increasing the strength of the material.

3.2 Microstructural characterisation

3.2.1 SEM characterisation of as-sprayed samples

This section presents results obtained from the microstructural characterisation of as-sprayed samples using the SE imaging mode in the SEM. Figure 6 shows the SEM micrographs of as-sprayed MCS samples. The red arrow in Figure 6 (a) represents a view perpendicular to the surface of the coating layer, whereas the green arrow represents a view perpendicular to the cross-section of the sample. The microstructures in Figures 6(b-e) are viewed according to the direction of the green arrow, whereas Figure 6(f) is viewed according to the direction of the red arrow. The morphology of constituent layers of as-sprayed samples is shown in Figure 6(b), which depicts the deformed appearance of powder particles. Individual particles are clearly separated by boundaries. According to Figure 6(c), the substrate layer shows a typical duplex microstructure in Ti-6Al-4V, which contains near equiaxed primary α grains and lamellar secondary α within β matrix. The duplex microstructure gives the alloy well-balanced mechanical properties. This is because equiaxed microstructures usually provide good ductility and fatigue strength, whereas lamellar microstructures enhance the fracture toughness, resistance to fatigue crack growth and creep of the alloy. An interesting feature in Figure 6(d) is shown by the appearance of small, irregular-shaped particles surrounded by larger particles in the microstructure (see yellow arrow). Identical observations have also been made at other regions in the coating layer of the sample. While the exact reasons for these observations are unknown, a possible explanation is that particles have broken into smaller fragments during impact on the substrate surface, which then compacted tightly together as successive layers of particles were sprayed. According to Assadi et al. [3], particle impact during the deposition process is related to the viscoplastic deformation of feedstock powder particles, which leads to two phenomena. The first is the compaction of particles into a deposit, and the second is the formation of bonds between particles themselves. These processes will influence the density and strength of the deposit. An in-depth explanation about the underlying physics of the particle impact and deformation is described in published literature by Assadi et al. [3]; the same author(s) also explored the optimisation of the cold spray process based on different parameters using an integrated experimental-numerical approach in [10]. Another notable feature of the coating surface are crevices such as those in Figures 6(d) and (e), where the spherical outline of powder particles can be seen (see black arrows) inside the crevices. As mentioned earlier, particles are sprayed onto the substrate surface at a temperature below their melting point in the cold spray process, and they bond due to plastic deformation. Hence, they are still visible in the microstructure as they have not melted. In Figure 6(f), an acicular morphology can be observed in the particle, which is in good agreement with findings published in [11]. Micro-porosities (see black arrows) are also located along the boundaries between particles.
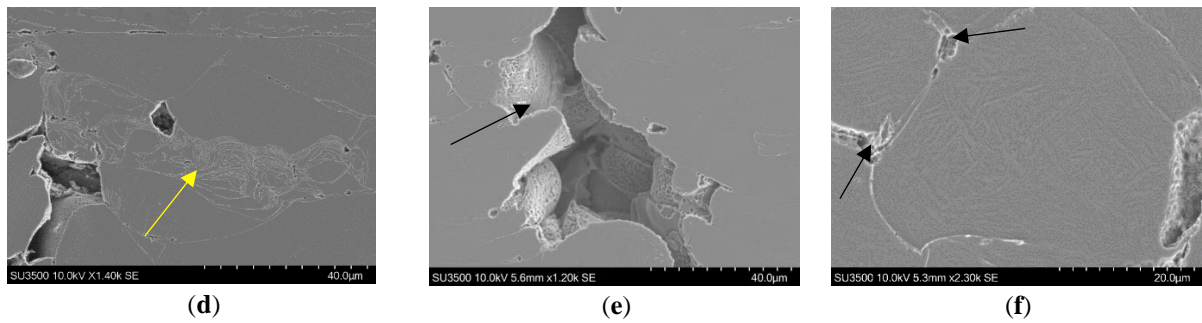

(a)   (b)   (c)

(**d**)   (**e**)   (**f**)
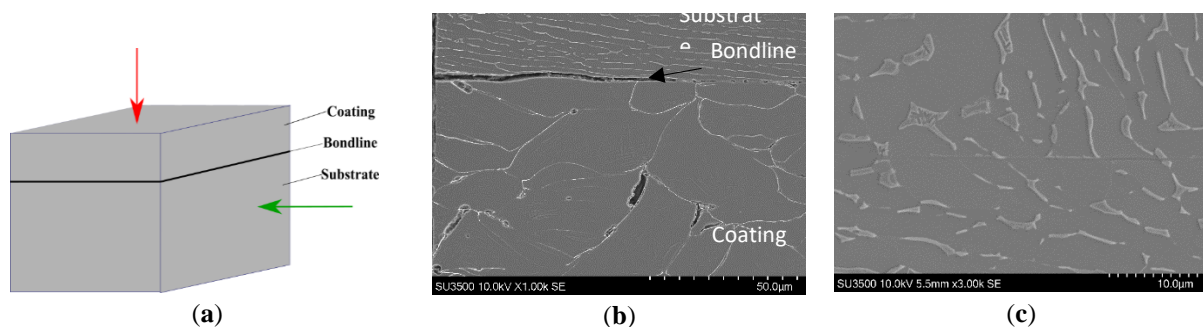
Figure 6. SEM micrographs of as-sprayed samples; (**a**) Schematic of viewing directions on samples, (**b**) Region showing the substrate, bondline and coating layers, (**c**) Substrate layer, (**d**) Coating layer, (**e**) Cavity in coating layer, (**f**) Acicular morphology and porosities in coating layer.

3.2.2 Porosity analysis of as-sprayed samples

This section presents results from the porosity analysis of as-sprayed samples. The analysis is performed by obtaining optical micrographs of samples in the unetched condition, followed by image processing of the micrographs using ImageJ. Samples were analysed in the unetched condition so that porosities can be clearly detected without being masked by features revealed from etching such as grain boundaries. The faint bands observed in Figure 7(a) are scan marks from the image stitching process in the Smartzoom microscope that do not affect the porosity analysis of the sample. In ImageJ, the first step for image processing is converting the optical micrographs into binary images. Statistical tools in the software are then used to measure the area of porosities [12]. In order to distinguish real porosities from other features in the microstructure, the software is set to detect objects with a circularity of 0.2-1, where values of 0 and 1 represent a perfect line and a perfect sphere respectively. The outlines of detected objects are displayed. An example is given in Figure 7(b), which shows the magnified image of the region highlighted (see red square) in Figure 7(a). The same procedures were repeated when analysing the porosities in sample 4. However, only the coating layer is analysed as the substrate layer contains a negligible amount of porosities. In Figure 7(c), the area highlighted by the red square is magnified and shown in Figure 7(d).

(**a**)   (**b**)

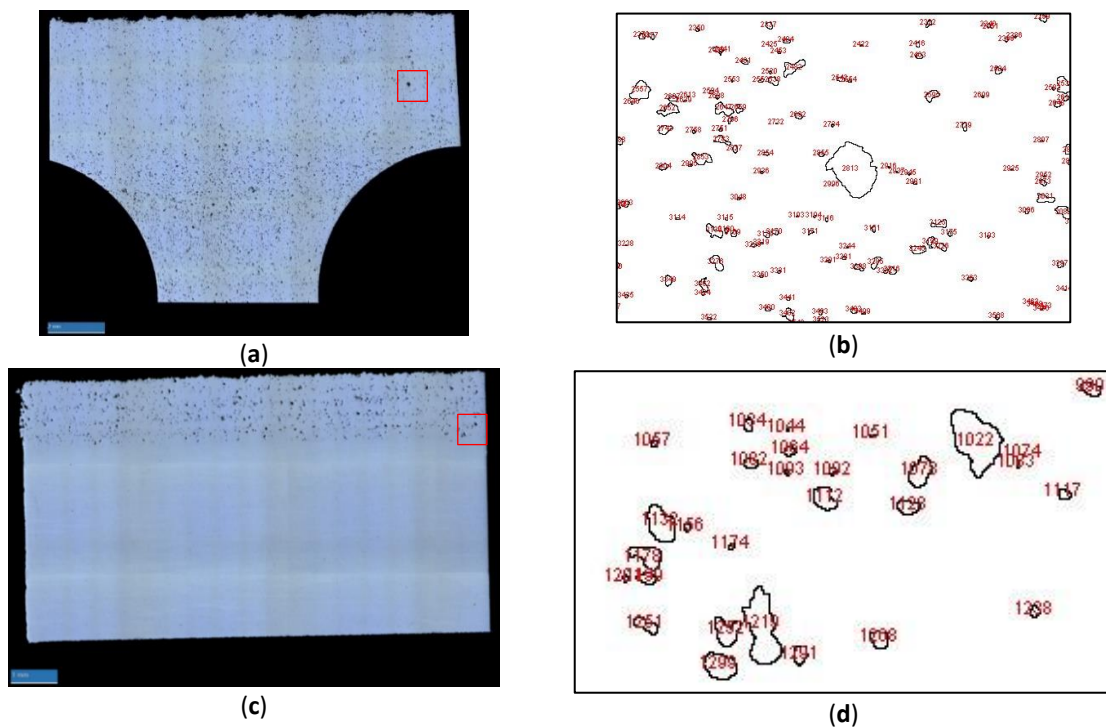(**c**)   (**d**)

Figure 7. Optical micrographs for porosity analysis in as-sprayed samples; (**a**) Micrograph of sample 8b in unetched condition (viewed perpendicular to coating layer), (**b**) Processed image of sample 8b on ImageJ, (**c**) Micrograph of sample 4 in unetched condition (viewed perpendicular to cross-section of sample), (**d**) Processed image of sample 4 on ImageJ.

Quantifiable data associated with the porosity analysis of as-sprayed samples is presented in Table 2. Samples 1 and 8b are those that are viewed perpendicular to the coating layer, whereas samples 4 and 7 are viewed perpendicular to the cross-section of the sample. Several trends in the size of porosities can be drawn from Table 2. For instance, the average area analysed is approximately 10-4 mm2; the maximum area is approximately between 10-3 -10-2 mm2; and the minimum area is approximately 10-6 mm2. It is clear that the sizes of porosities can vary quite significantly, which correlates to Figure 15(b). The percentage porosity is calculated using the following formula:

$$Percentage\ porosity = \frac{Total\ area\ occupied\ by\ porosities}{Area\ of\ region\ analysed\ on\ the\ image} \times 100\%. \qquad (1)$$

The percentage porosity of all samples were found to be below 10%. A primary reason for the formation of pores in the coating layer is due to the entrapment of air as a result of the high surface reactivity between titanium powder particles and oxygen [13]. A highly porous structure may also form if there is inadequate deformation between interacting particles as a result of low deposition velocity [3, 14]. Although the process parameters affecting porosity are not studied in detail in this paper, it is vital to understand their relationship as it influences the mechanical properties of cold spray samples. For example, it has previously been found that coating microhardness can be enhanced when porosity levels are reduced via an increase in deposition velocity [11, 15-16]. The effect of powder morphology on porosity was investigated by Wong et al. [15]. The type of deposition gas also affects the porosity level, where Zahiri and co-workers [16] discovered that the use of helium gas greatly reduces the volume fraction of porosities. Other important factors that affect porosity include powder flight distance, powder sizes, gas pressure and temperature [16]. It should be noted that the porosity analysis method used in this study gives a relatively simple representation of the porosity levels in as-sprayed samples. The accuracy of the data can be improved by using methods such as the ASTM C20:2000 standard, which was implemented to measure the porosity levels in commercially pure titanium cold spray samples in [16].

Lastly, the substrate layer in Figure 16(c) shows virtually no evidence of porosity. Based on this observation, results from the porosity analysis are in good agreement with those presented in Figure 3, where the peak loads of bondline samples are higher than those of coating samples. The coating layer is brittle due to high amounts of porosity. Therefore, the presence of the substrate layer will engender more strength to the cold spray sample.

Table 2. Porosity analysis data.

Item	Sample 1	Sample 8b	Sample 4	Sample 7
Number of porosities	38894	13334	1418	9121
Area of sample (mm^2)	138.19	104.43	53.70	89.99
Average area of porosity (mm^2)	3.45×10^{-4}	3.28×10^{-4}	2.95×10^{-4}	2.40×10^{-4}
Maximum area of porosity (mm^2)	1.30×10^{-2}	1.30×10^{-2}	3.00×10^{-3}	7.00×10^{-3}
Minimum area of porosity (mm^2)	4.80×10^{-6}	4.84×10^{-6}	4.79×10^{-6}	4.81×10^{-6}
Area of region analysed on the image (mm^2)	138.19	104.43	14.20*	22.74*
Total area occupied by porosities (mm^2)	13.42	4.37	0.42	2.19
Percentage porosity (%)	9.71	4.18	2.96	9.63

* *Since samples 4 and 7 are viewed perpendicular to the cross-section (i.e. showing the coating, bondline and substrate layers), the area of analysis is restricted only to the coating layer so that the porosity analysis is performed consistently with samples 1 and 8b (i.e. which are viewed perpendicular to the coating layer).*

4. Conclusions

The failure modes of cold spray Ti-6Al-4V coating on a TI-6Al-4V substrate has been studied and elucidated in this paper. A series of SP tests have been performed, followed by fractographic investigations. Additional material characterisation has also been performed to gain a better understanding of the cold-sprayed microstructure. The following conclusions can be drawn from this study:

1. SP tests have shown that coating samples displayed a brittle behaviour and could withstand the least peak load, whereas substrate samples showed reasonable ductility and were able to withstand the highest peak load among all samples. Bondline specimens displayed the most ductile behaviour and could sustain a moderate peak load.

2. At different temperature, the bondline samples tend to show a variance in ductility. Ductility was found to increase with temperature, which enabled them to plastically deform to a greater extent and withstand higher load.

3. SEM characterisation of SP specimens has shown that coating samples failed in a brittle manner since they display a flat crack surface with facets while substrate samples exhibit a more ductile, dimple type fracture due to the formation of microvoids which eventually grow and coalesce. Bondline samples exhibit both ductile and brittle fracture surfaces. The increase in temperature was found to cause the detachment of the coating layer from the sample.

4. The deformed morphology of powder particles in as-sprayed samples are in good agreement with plastic deformation mechanisms for particle-particle and particle-substrate bonding as reported in published literature.

5. The size of porosities in as-sprayed samples followed a certain trend: (i) The maximum area of porosities were approximately 10^{-3}-10^{-2} mm^2, (ii) the minimum area of porosities were approximately 10^{-6} mm^2, and (iii) the average area of porosities were approximately 10^{-4} mm^2. Additionally, the level of porosity in the coating of as-sprayed Ti-6Al-4V material was found to be consistently above approximately 3% and is expected to have a strong influence on the mechanical performance of such materials.

References

1. Singh, H.; Sidhu, T.S.; Kalsi, S.B.S. Cold spray technology: future of coating deposition processes, *Frattura ed Integrità Strutturale* **2012**, *6*, 69-84, DOI: 10.3221/IGF-ESIS.22.08.

2. Khun, N.W.; Tan, A.W.Y.; Liu, E. Mechanical and tribological properties of cold-sprayed Ti coatings on Ti-6Al-4V substrates, *J. Therm. Spray Tech.* **2016**, *25*, 715-724, DOI: 10.1007/s11666-016-0396-6.

3. Assadi, H.; Kreye, H.; Gärtner; F.; Klassen. T. Cold spraying – A materials perspective, *A. Materialia* **2016**, *116*, 382-407, DOI: 10.1016/j.actamat.2016.06.034.

4. Henao, J.; Sharma. M.M. Characterization, Deposition Mechanisms, and Modeling of Metallic Glass Powders for Cold Spray. In *Cold-Spray Coatings: Recent trends and future perspectives*, 1st ed.; Cavaliere, P., Ed.; Springer: Cham, Switzerland, **2018**; pp. 251-272, ISBN: 978-3-319-67183-3.

5. IIIsley, H.; Lancaster, R.J; Hurst, R.C.; Jeffs, S.P.; Baxter. G. Mechanical property characterisation of electron beam melted (EBM) Ti-6Al-4V via small punch tensile testing, Proceedings of the 4th International Conference on Small Scale Test Techniques, Shanghai, China, Oct 12-14; Guan, K., Matocha, K., Xu, T., Eds.; Trans Tech Publications: Zurich, Switzerland, 2016.

6. CEN Workshop Agreement CWA 15627, European Code of Practise: Small Punch Test Method for Metallic Materials. (2007).

7. Davies, S.; Lancaster, R.; Jeffs, S.; Baxter. G. Small Punch Testing of Powder Bed Direct Laser Deposits, Proceedings of the 4th International Conference on Small Scale Test Techniques, Shanghai, China, Oct 12-14; Guan, K., Matocha, K., Xu, T., Eds.; Trans Tech Publications: Zurich, Switzerland, 2016.

8. Parrington, R.J. Fractographic Features in Metals and Plastics. *Adv. Mater. Process* **2003**, 161, 37–40.

9. Becker, W.T.; Lampman, S. Fracture Appearance and Mechanisms of Deformation and Fracture. *ASM Handb.*, **2012**, 11, 559–586.

10. Assadi, H.; Schmidt, T.; Richter, H.; Kliemann, J.O.; Binder, K.; Gärtner, F.; Klassen, T.; Kreye, H.; On Parameter Selection in Cold Spraying, *J. Therm. Spray Tech.*, **2011**, *20*, 1161-1176, DOI: 10.1007/s11666-011-9662-9.

11. Ajaja, J.; Goldbaum, D.; Chromik, R.R. Characterisation of Ti cold spray coatings by indentation methods, *A. Astronautica.*, **2011**, *69*, 923-928, DOI: 10.1016/j.actaastro.2011.06.012.

12. Moy, C.K.S.; Cairney, J.; Ranzi, G.; Jahedi, M.; Ringer. S.P. Investigating the microstructure and composition of cold gas-dynamic spray (CGDS) Ti powder deposited on Al 6063 substrate, *Surface and Coatings Technology*, **2010**, *204*, 3739-3749, DOI: 10.1016/j.surfcoat.2010.04.016.

13. Li, W.Y.; Zhang, C.; Wang, H.T.; Guo, X.P.; Liao, H.L.; Li, C.J.; Coddet, C. Significant influences of metal reactivity and oxide films at particle surfaces on coating microstructure in cold spraying, *Applied Surface Science*, **2007**, *253*, 3557-3562, DOI: 10.1016/j.apsusc.2006.07.063.

14. Ogawa, K.; Seo, D. Repair of Turbine Blades Using Cold Spray Technique. In *Advances in Gas Turbine Technology*, 1st ed.; Benini, E. Ed.; InTech: London, United Kingdom, 2011; pp. 499-526, ISBN: 978-953-307-611-9.

15. Wong, W.; Rezaeian, A.; Irissou, E.; Legoux, J.G.; Yue. S. Cold spray characteristics of commercially pure Ti and Ti-6Al-4V, *Adv. Mater. Research*, **2010**, *89-91*, pp 639-644, DOI: 10.4028/www.scientific.net/AMR.89-91.639.

16. Zahiri, S.H.; Antonio, C.I.; Jahedi. M. Elimination of porosity in directly fabricated titanium via cold gas dynamic spraying, *Journal of Materials Processing Technology*, **2009**, *209*, 922-929, DOI: 10.1016/j.jmatprotec.2008.03.005.